MICROWAVE SCATTERING MODELS AND BASIC EXPERIMENTS

Prepared for

National Aeronautics and Space Administration
Goddard Space Flight Center
Greenbelt, Maryland 20771

Grant NAG 5-486

Final report for the period: November 1, 1986 - April 30, 1989

by

Adrian K. Fung

Wave Scattering Research Center
University of Texas at Arlington
Arlington, Texas 76019

ABSTRACT

This final report summarizes progresses made in the four proposed areas of study: (1) scattering model development for sparsely populated media, such as a forested area; (2) scattering model development for dense media, such as a sea ice medium or a snow covered terrain; (3) model development for randomly rough surfaces; and (4) design and conduct of basic scattering and attenuation experiments suitable for the verification of theoretical models. Progress during the course of this research has been detailed in semi-annual reports and forwarded to NASA. Hence, only the final results in each category are given in this report.

1. INTRODUCTION

A scattering model has been developed for a deciduous and/or a coniferous forested area. The components of the forest consist of leaves, branches, trunks, and a rough ground surface. These components are modeled respectively as needles or elliptic discs with various ellipticities, dielectric cylinders of finite length, large vertical dielectric cylinders, and an irregular, finitely conducting ground surface. Typical predictions of this model are given in the next section and a detailed model development is given in Karam and Fung [1989]. Other related studies include permitting near field interaction between scatterers [Fung, Chen and Lee, 1986], leaf shape effects [Karam et al, 1988], extinction coefficients in forested areas [Karam et al, 1988], scattering properties of vegetation components [Karam, Fung and Antar, 1988], scattering from a layer of defoliated vegetation [Karam and Fung, 1988], empirical modeling of a vegetation layer [Liu and Fung, 1988], and emissions from a multi-layered random medium [Karam and Fung, 1986].

A new approach has been applied to develop a dense medium scattering model and applied to scattering from a snow covered surface [Fung and Chen, 1988]. This approach is based on the Helmholtz integral representation for the scattered field in terms of the field inside the scatterer. A pair correlation function accounting for the spatial distribution of scatterers is used to describe the nature of the dense medium. The general behavior of this model as a function of volume fraction and the size of the scatterer is illustrated in Section 3. Its application to imaging is discussed in Fung, [1988].

A rough surface backscattering model valid over the entire frequency range has been developed for a randomly rough, perfectly conducting surface [Fung and Pan, 1987]. Its range of validity has been determined and shown to be valid for a moderately rough continuous surface [Pan and Fung, 1987]. The surface rms slope should be less than 0.4. A summary of the predictions of this model is given in Section 4.

Experimental studies have been carried out in the generation of known rough surfaces [Rochier et al, 1988] for scattering measurements, polarimetric microwave scattering measurements from known rough surfaces [Blanchard, Nance and Chen, 1988], attenuation and scattering measurements from a dense medium [Blanchard, Syed and Fung, 1988], and bistatic microwave measurements of simulated natural structures [Blanchard and Nance, 1988]. Results of these studies have been included in the semi-annual report for the period May 1, 1988 to October 31, 1988 and, hence, will not be repeated here.

2. Behaviors of a Scattering Model for a Forested Area

In this forest scattering model four major scattering mechanisms are included: scattering by the ground surface attenuated by the vegetation layer; volume scattering from the crown layer including leaves and branches; trunk-surface interaction attenuated by the crown layer; and surface-crown layer interaction. In what follows illustrations of these scattering mechanisms are shown for incident plane wave with q polarization ($q=v_i$ or h_i) and in θ_i direction (θ_i is measured from the normal to the canopy).

2.1 Ground Surface Scattering

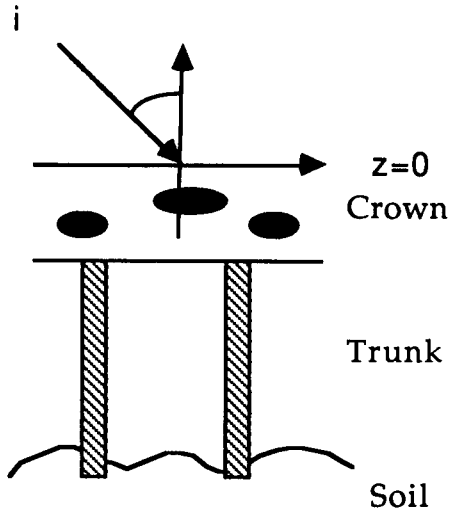

Figure 2.1 Scattering Geometry

For the scattering geometry in Figure 2.1, the backscattering coefficient due to the surface scattering can be written as [Karam and Fung, 1989a]

$$\sigma^0_{pq}(s) = L_{1p}\, L_{2p}\, R_{pq}\, L_{1q}\, L_{2q} \qquad (2.1)$$

Where p is the scattered field polarization ($q=v_s$ or h_s) and R_{pq} is the surface backscattering coefficient. L_{1q} and L_{2q} are the crown and the trunk loss factors which have H_1 and H_2 depth respectively

$$L_{1p} = e^{-[k_{1p} H_1 \sec\theta_i]}$$
$$L_{2p} = e^{-[k_{2p} H_2 \sec\theta_i]} \qquad (2.2)$$

and k_{1p} and k_{2p} are the crown and trunk extinction coefficient respectively [Karam et al, 1988b; Karam and Fung, 1989c].

2.2 The Crown Scattering

The crown backscattering coefficient can be written as

$$\sigma^0_{pq}(c)=4\pi \cos\theta_i \{n_L<|F_{Lpq}|^2> + n_b <|F_{bpq}|^2>\} \left\{\frac{1-L_{1p} L_{1q}}{k_{1p} + k_{1q}}\right\} \qquad (2.3)$$

where n_L and n_b are the leaf and the branch number densities. F_{Lpq} and F_{bpq} are the scattering amplitude tensors for leaves and branches in the backward direction [Karam and Fung, 1988, 1989b]. The ensemble average < > is taken over the leaf and the branch orientations.

2.3 The Crown-surface Scattering

The crown-surface interaction backscattering coefficient is

$$\sigma^0_{pq}(c \leftrightarrow s)= \sigma^0_{pq}(c \rightarrow s) +\sigma^0_{pq}(s \rightarrow c) \qquad (2.4)$$

The first term in (2.4) is due to scattering from the crown followed by scattering from the surface. The second term is due to scattering from the surface followed by scattering from the crown. The explicit contents of these terms are

$$\sigma^0_{pq}(c \rightarrow s) = 4\pi \cos\theta_i L_{1p} L_{2p} \left\{\frac{L_{1p} - L_{1q}}{k_{1q} - k_{1p}}\right\} R'_{pp} L_{2p}$$
$$\{n_L<|F'_{Lpq}|^2> + n_b <|F'_{bpq}|^2>\} \qquad (2.5)$$

$$\sigma^0_{pq}(s \rightarrow c) = 4\pi \cos\theta_i \left\{ \frac{L_{1p} - L_{1q}}{k_{1q} - k_{1p}} \right\} L_{2q} \; R'_{qq} \, L_{1q} \, L_{2q}$$
$$\{n_L < |F'_{Lpq}|^2 > + \; n_b < |F'_{bpq}|^2 >\} \qquad (2.6)$$

where R'_{pp} is the Fresnel reflectivity. F'_{Lpq} and F'_{bpq} are the scattering amplitudes in the specular direction [Karam and Fung, 1988, 1989; Karam et al, 1989b].

When p=q, (2.5) and (2.6) reduce to

$$\sigma^0_{pp}(c \rightarrow s) = \sigma^0_{pp}(s \rightarrow c) = 4\pi H_1 \, L^2_{1p} \, L^2_{2p}$$
$$\cdot \{n_L < |F'_{Lpq}|^2 > + \; n_b < |F'_{bpq}|^2 >\} R'_{pp} \qquad (2.7)$$

2.4 Trunk-surface Scattering

The trunk-surface backscattering coefficient is equal to

$$\sigma^0_{pq}(t \leftrightarrow s) = \sigma^0_{pq}(t \rightarrow s) + \sigma^0_{pq}(s \rightarrow t) \qquad (2.8)$$

The first term is due to scattering from the trunk followed by scattering from the surface. The second term is due to scattering from the surface followed by scattering from the trunk. Since the trunks have dimensions larger than the incident wavelength, the cross-polarized component vanishes and the like cross-polarized component can be written as

$$\sigma^0_{pp}(t \rightarrow s) = \sigma^0_{pp}(s \rightarrow t) = 4\pi \; H_2 \; n_t \; [L_{1p} \, L_{2p}]^2 \; |F'_{tpp}|^2 \; R'_{pp} \qquad (2.9)$$

where n_t is the trunk number density. F'_{tpp} is the trunk scattering amplitude in the specular direction.

2.5 Results and Discussions

Figures 2-7 are presented here to illustrate the contribution of each term to the total backscattering coefficient and the relative values of the like and cross-polarized coefficients. In these figures, the branches are modeled by randomly oriented, finite-length cylinders, and the leaves are modeled by randomly oriented circular discs. The

cylinder and the disc orientations are described by the Eularian angles of orientation (α, β, γ). Due to the scatterer symmetry, the third angle of orientation γ has no effect on the scattering coefficient.

The selected cylinder parameters are as follows: a (radius) = 2.5 cm, h (length/2) = 20cm, $0^o < \alpha < 360^o$; $10^o < \beta < 70^o$; $\varepsilon_r = 12.4 - j4.9$; v_f (volume fraction) = 0.1×10^{-2}. The selected disc parameters are as follows: a (radius) = 2 cm, h (thickness/2) = 0.125 mm; $0^o < \alpha < 360^o$; $60^o < \beta < 90^o$; m_g (gravimetric leaf moisture) = 0.46. The trunks are modeled by vertical cylinders with parameters: a (radius) = 12cm; H_2 (length) = 10 m; $\varepsilon_r = 12.4 - j4.9$; n_t (number density per unit area) = 0.11 m^{-2}.

The figures illustrate the backscattering coefficients as a function of the incident angles at three different frequencies.

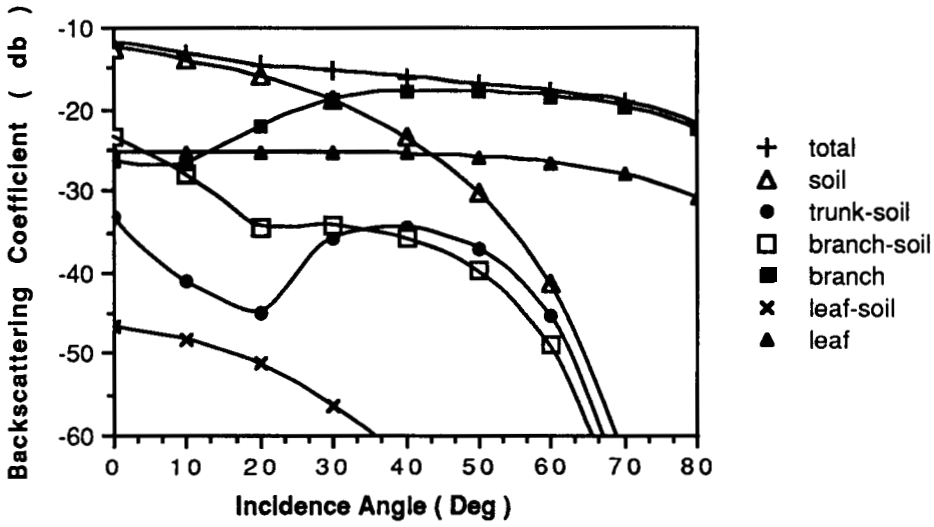

Figure 2.2 The VV backscattering coefficient components for a forested canopy at L band (F = 1.5 Ghz)

Figures 2.2 and 2.3 show the backscattering coefficient at 1.5 GHz. The dominant contributing term at small angles of incidence is from the ground, and at larger angles of incidence it is the volume scattering due to branches which dominates. Other terms are less important with the choice of parameters indicated. Figure 2.3 shows that the cross-polarization is due mainly to branches at this frequency.

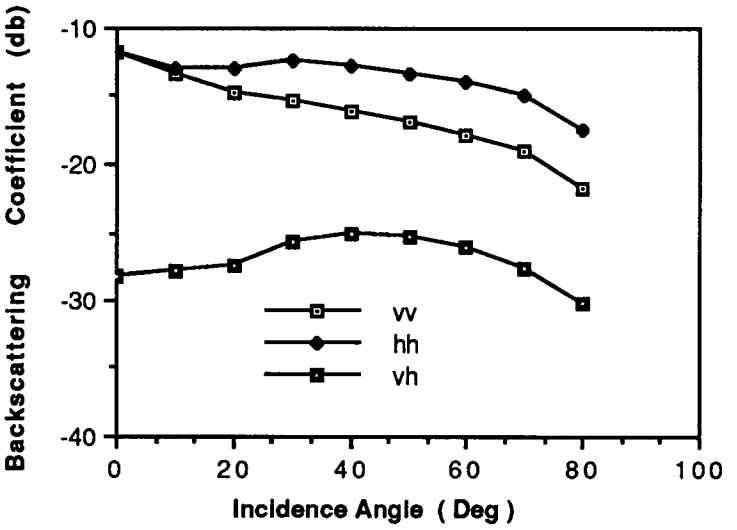

Figure 2.3 The like and cross backscattering coefficient from a forested canopy at L band (F = 1.5GHz)

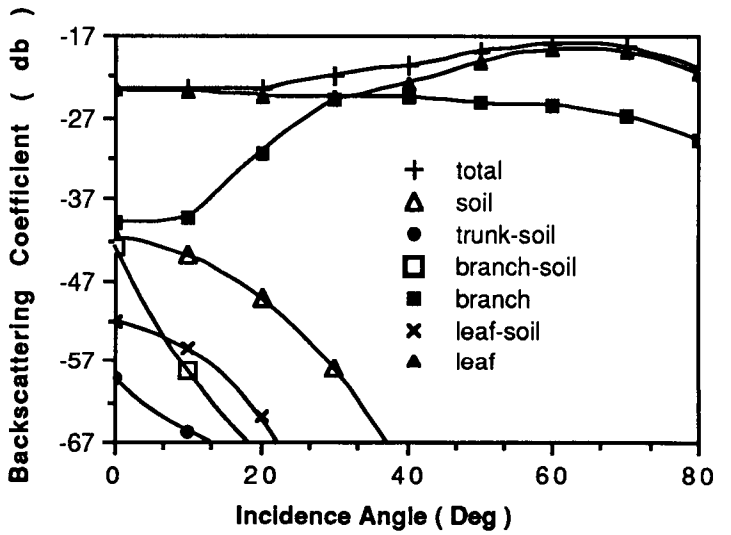

Figure 2.4 The VV backscattering coefficient components for a forested canopy at C band (F=6.5Ghz)

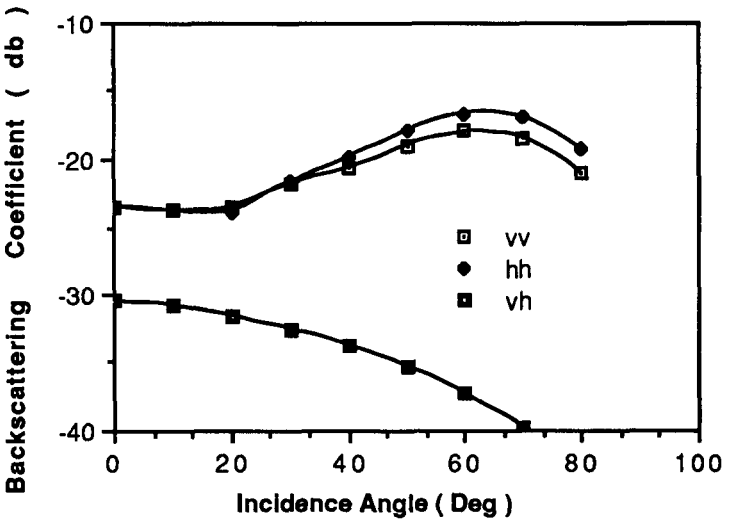

Figure 2.5 The like and cross backscattering coefficients for a forested canopy at L band (F=6.5 Ghz)

Figures 2.4 and 2.5 show similar calculations for the backscattering coefficients at 6.5 GHz. Here the dominant contribution comes from leaves, with contribution from branches as a secondary factor. When frequency is further increased to 10 GHz we see from Figures 2.6 and 2.7 that the dominant contribution is from leaves.

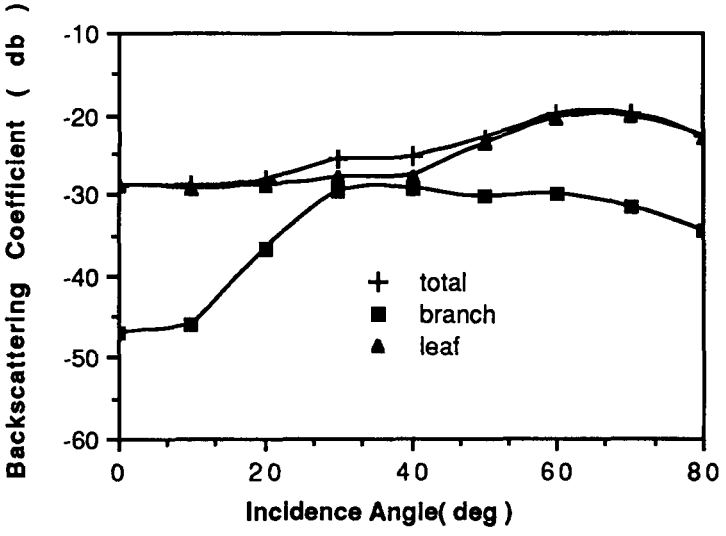

Figure 2.6 The backscattering coefficient (vv) components for a forested canopy at X band (F=10 Ghz)

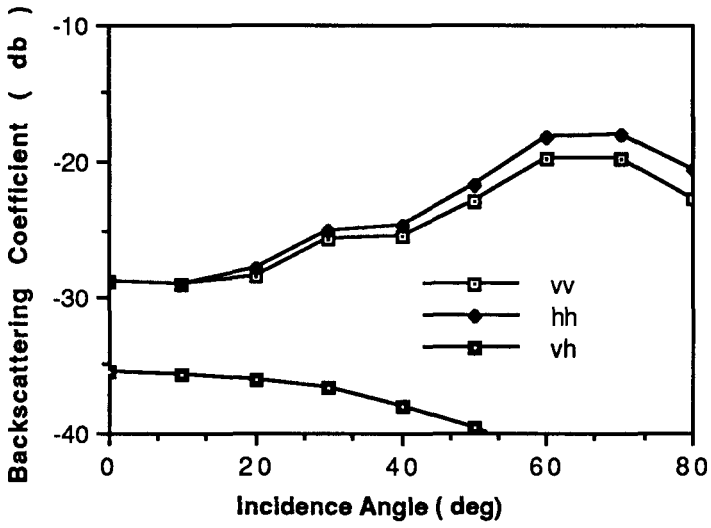

Figure 2.7 The like and cross backscattering coefficients for a forested canopy at X band (F= 10 ghz)

3. Behaviors of a Dense Medium Scattering Model

In this section the theoretical results of a model for dense medium scattering is summarized. To demonstrate the scattering properties of the model, the simple case of scattering from a half space medium with densely packed spherical scatterers is considered.

3.1 The Backscattering Coefficient

This dense medium scattering model is based on the Helmholtz integral formulation for the scattered field in terms of the field inside the scatterer. The pair correlation between scatterers used to characterize the dense medium effect comes in when ensemble averaging is performed on the scattered field product to obtain the average power. The backscattering coefficient is given as

$$\sigma^0_{pp} = 4\pi\, k_0^2 \cos\theta_s\, f(u,v)|_{u=k_0\sin\theta_s, v=0} \qquad (3.1)$$

where

$$f(u,v)= \frac{n_0\, 8\pi^2 |\beta|^2\, D}{|k'_e + k'_z|^2\,(k_{ei}\cos\theta_t + k'_{ei})}\ , \tag{3.2}$$

$$\beta = j\frac{3}{8\pi^2} k_0^2\, v_0\, T_p\, \frac{y}{1-fy} \tag{3.3}$$

In equation (3.3), v_0 is the volume of each particle; T_p is the p-polarized Fresnel transmission coefficient, f is the volume fraction of scatterers; k_0 is the wave number in free space and $y = (\varepsilon_{ice} - \varepsilon_{snow})/(\varepsilon_{ice} + 2\varepsilon_{snow})$. In equation (3.2), n_0 is the number density of the particles, θ_t is the angle of transmission between the air and the medium with a plane interface; and k_e is the effective wave number of the scattering medium. The definition of other variables in the expression of f(u,v) are,

$$k'_e = \sqrt{k_e^2 - u^2 - v^2},\ k'_z = \sqrt{k_0^2 - u^2 - v^2},\ k'_{ei} = \mathrm{Im}\{k'_e\},\ k_{ei} = \mathrm{Im}\{k_e\}.$$

For the sake of simplicity, the effective wave number k_e is evaluated in accordance with the empirical formula of snow derived by Hallikainen [1987]. Note that the solution given in (3.1) is for single incoherent scattering only. Multiple scattering can be included by the matrix doubling technique. The dense medium scattering phase matrix needed in the matrix doubling can also be developed in a similar manner.

The quantity D in (3.2) which accounts for the dense medium effect is obtained from averaging the scattered power. The process of averaging generates the "pair correlation function $\rho(\xi_x,\xi_y,\xi_z)$" of the scatterers.

$$D = 1 + n_0 \int \rho(\xi_x,\xi_y,\xi_z)\, e^{-j\vec{k}\cdot\vec{\xi}}\, d\vec{\xi} \tag{3.4}$$

where

$$\vec{k} = \hat{x}\,(k_0\sin\theta + u) + \hat{y}\, v - \hat{z}\,(k_{er}\cos\theta_t + k'_{er})$$

$$\vec{\xi} = \hat{x}\,\xi_x + \hat{y}\xi_y + \hat{z}\xi_z.$$

Note that k_{er} and k'_{er} are the real part of k_e and k'_e respectively.

Assuming an exponential, isotropic correlation function $\rho(r) = e^{-r/L}$, the dense medium factor D in the backscattered direction can be integrated as

$$D = 1 + \frac{4\pi n_0 L^2}{|K} \frac{e^{-2a/L}}{1+(|K\,L)^2}\left[\left(2\,|Ka + \frac{2\,|K\,L}{1+(|K\,L)^2}\right)\cos(2\,|K\,a) + \left(\frac{2a}{L} + \frac{1-(|K\,L)^2}{1+(|K\,L)^2}\right)\sin(2\,|K\,a)\right] \tag{3.5}$$

where "a" is the radius of the scatterers and $|K=[4k_0^2 \sin^2\theta + (k_{er}\cos\theta_t + k'_{er})^2]^{1/2}$.

3.2 Theoretical Results

In this section the effect of volume fraction, particle size, frequency, liquid water content, and correlation length on the backscattering coefficient of snow are presented.

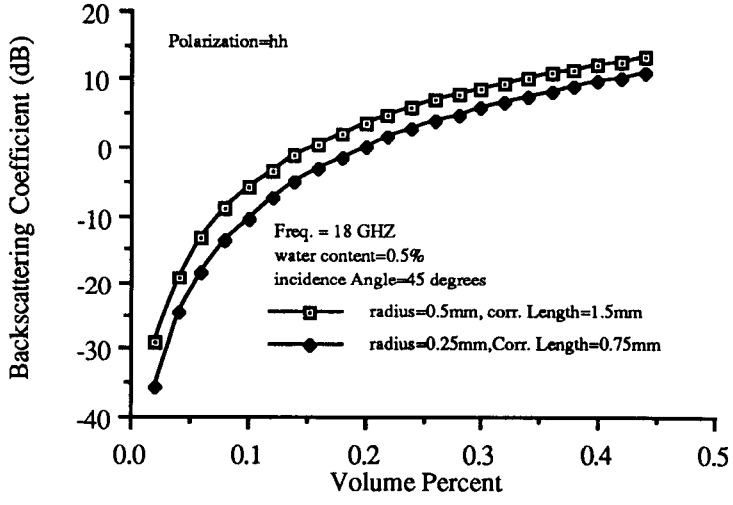

Figure 3.1 The effect of volume fraction of scatterers on the backscattering coefficient of snow.

In Figure 3.1, the hh polarized backscattering coefficient at 45 degrees incidence angle and 18 GHz is plotted versus increasing volume percent of the scatterers for two particle sizes. The correlation length is chosen to be three times the particle radius for

each case. It is seen that the effect of increasing volume percent is to increase the scattering for both particle sizes. In the modeling of scattering from snow using either the Rayleigh or the Mie scattering model under the assumption that the particles are far apart from each other, unreasonably large particle size must be used to fit the level of the data. It is anticipated that the effect of closely packed scatterers is to increase the scattering such that smaller particle size can be used to realize the data fit. The increasing trend of scattering coefficient versus volume fraction observed in Figure 3.1 agrees with this effect.

In Figure 3.2, the hh polarized backscattering coefficient versus frequency is plotted. The angle of incidence is 45 degrees, the volume fraction is 30%, the liquid water content is 0.5%. Two different particle radii, 0.25 and 0.5 mm, are plotted. The correlation length is again chosen to be three times the radius. It is seen that the effect of increasing frequency is to increase scattering.

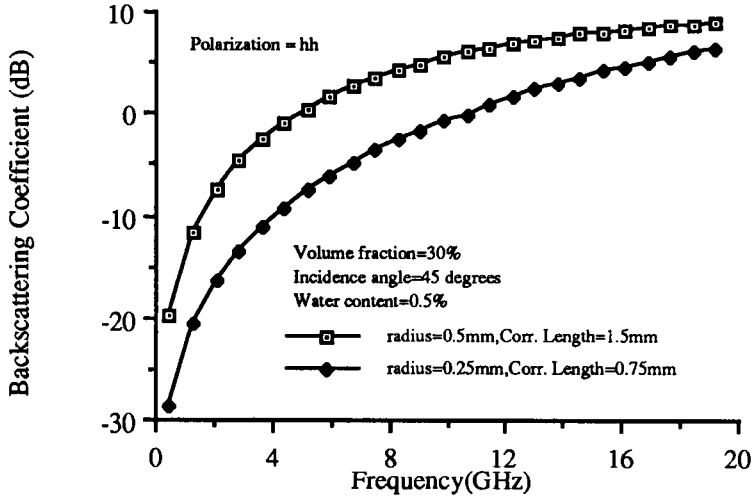

Figure 3.2 The effect of frequency on the backscattering coefficient of snow.

In Figure 3.3, the effect of liquid water content on the backscattering coefficient from snow is plotted for hh polarization at the angle of incidence of 45 degrees. The volume fraction of the scatterers is 30%, particle radius is 0.5 mm, and the correlation length is 1.5 mm. The effect of increasing water content is to increase absorption. The effect of increasing absorption is to decrease the scattering albedo. Decreasing the albedo causes a decrease in the scattering coefficient. This phenomenon is clearly demonstrated in Figure 3.3 for two frequencies, 9 and 18 GHz.

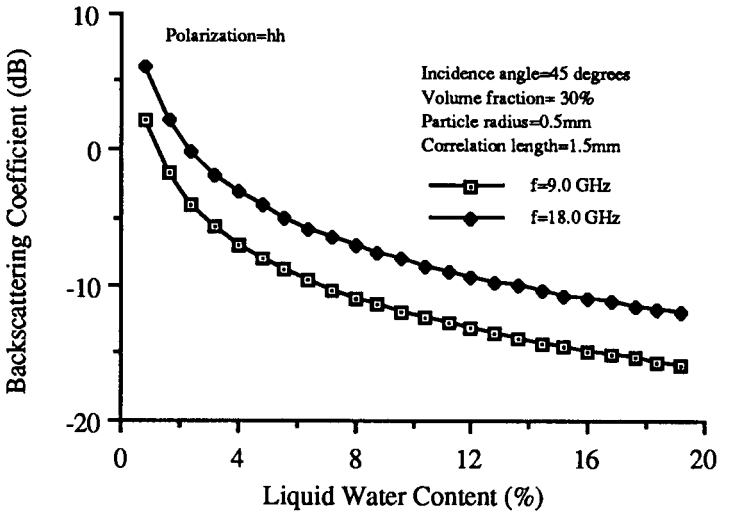

Figure 3.3 The effect of liquid water content on the backscattering coefficient of snow.

In Figure 3.4, the effect of the correlation length of the pair correlation function on the backscattering coefficient is plotted. The angle of incidence is 45 degrees, volume fraction is 30%, liquid water content is 0.5%, and the particle radius is 0.5 mm. Scattering coefficients at four frequencies, 3.0, 7.5, 18.0 and 25.0 GHz, are plotted in Figure 3.4.

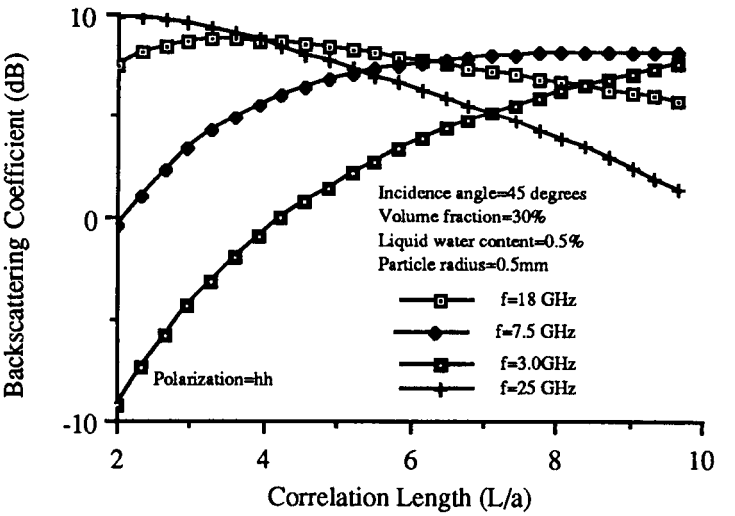

Figure 3.4 The effect of the correlation length of pair correlation on the backscattering coefficient of snow.

It is seen that at low frequencies of 3.0 and 7.5 GHz, the effect of increasing correlation length is to increase the scattering coefficient. At 25 GHz the trend reverses. At 18 GHz the trend is to first increase and then decrease as the correlation length increases. Actually, the 3.0 and 7.5 GHz curves eventually decrease at a much larger value of the correlation length. Also, the 25 GHz curve increases at small values of the correlation length. The phenomenon of increasing at small correlation values and decreasing at larger values is common to all frequencies and can be explained as a resonance effect. Depending on the frequency, the resonance occurs at different values of the correlation length.

4. A Summary of a Surface Scattering Model

In this section the results of the backscattering model by Fung and Pan [1987] are summarized and applied to investigate the polarization effects in rough surface scattering.

4.1 The Backscattering Coefficient

The vertically and horizontally polarized backscattering coefficients denoted by σ^0_{vv} and σ^0_{hh} for a randomly rough perfectly conducting surface with standard deviation σ and normalized roughness spectrum W(K) is

$$\sigma^0_{vv,hh} = (2k^2/\cos^2\theta)e^{-4k^2\sigma^2\cos^2\theta}\sum_{n=1}^{\infty}[(4k^2\sigma^2\cos^2\theta)^n/n!]W^{(n)}(2k\sin\theta,0)$$

$$\pm 4\sin^2\theta\, e^{-3k^2\sigma^2\cos^2\theta}\sum_{n=1}^{\infty}[(2k^2\sigma^2\cos^2\theta)^m/m!]W^{(m)}(2k\sin\theta,0)$$

$$+ 4\sin^4\theta e^{-2k^2\sigma^2\cos^2\theta}\sum_{n=1}^{\infty}[(k^2\sigma^2\cos^2\theta)^m/m!]W^{(m)}(2k\sin\theta,0) \qquad (4-1)$$

where k is the wave number; θ is the incidence angle; the minus sign in the middle term is for HH polarization; and $W^{(n)}$ (U,V) is the roughness spectrum of the surface related to the n^{th} power of the surface correlation function by the Fourier transform as follows:

$$W^{(n)}(U,V) = \frac{1}{2\pi}\int_{-\infty}^{\infty} e^{-jU\xi - jV\zeta}\rho^n(\xi,\zeta)\, d\xi d\zeta, \qquad (n=1,2,....)$$

Note that the first term in (4.1) is the standard Kirchhoff term. It should be the only term left when we take the high frequency limit. This, indeed, is the case since the

exponential decay factor in front of the second and the third terms are larger than the corresponding increases in the infinite sums as the wave number increases. More specifically, the sum in the second term cannot increase faster than $\exp(3k^2\sigma^2\cos^2\theta)$ and, similarly, the sum in the third term cannot increase faster than $\exp(2k^2\sigma^2\cos^2\theta)$ as the wave number increases.

In the low frequency limit we need to take only the n = 1 term in (4.1) and approximate the exponential functions by unity yielding

$$\sigma^0_{vv,hh} = 8k^4\sigma^2\, W(2k\sin\theta,0)\cdot \begin{cases} (1+\sin^2\theta)^2, \text{ for vv polarization} \\ \\ \cos^4\theta \text{ , for hh polarization} \end{cases} \qquad (4.2)$$

which is exactly the same as the results derived from the first-order small perturbation theory.

As an example, for a Gaussian correlation function,

$$\rho^n(\xi,\zeta) = \exp[-(\xi^2+\zeta^2)/L^2]$$

(4.1) takes the form,

$$\sigma^0_{vv,hh} = (2kL/\cos\theta)^2\exp[-(2k\sigma\cos\theta)^2]\sum_{m=1}^{\infty}[(k\sigma\cos\theta)^{2m}/(m!m)]e^{-(kL\sin\theta)^2/m}$$
$$\{4^{m-1}\pm 2^m\sin^2\theta\,\exp(k\sigma\cos\theta)^2 + \sin^4\theta\,\exp[2(k\sigma\cos\theta)^2]\} \qquad (4.3)$$

The cross-polarized backscattering coefficient denoted by σ^0_{vh} is [Fung and Pan, 1987]

$$\sigma^0_{hv}=\sigma^0_{vh} = (8/\pi\cos^2\theta)e^{-2k^2\sigma^2\cos^2\theta}\sum_{m,n=1}^{\infty}\frac{(k^2\sigma^2\cos^2\theta)^{m+n}}{m!\,m}$$
$$\int dudv\,\frac{[u^2v^2W^{(m)}(k\sin\theta+u,v)\;W^{(n)}(k\sin\theta-u,-v)]}{k^2-u^2-v^2} \qquad (4.4)$$

It is easy to see that (4.4) vanishes in the high frequency limit due to the exponential decay factor. In the low frequency region we set m=n=1 and approximate $\exp(-2k^2\sigma^2\cos^2\theta)$ by unity yielding

$$\sigma^0_{hv} = \sigma^0_{vh} = \frac{8}{\pi} k^4 \sigma^4 \cos^4\theta \int dudv \frac{u^2 v^2 W(k\sin\theta+u,v)\, W(k\sin\theta-u,-v)}{(k^2-u^2-v^2)\cos^2\theta} \qquad (4.5)$$

This expression is in agreement with Rice [1951] and also Valenzuela [1967] if we let the relative dielectric constant approach infinity in Valenzuela [1967]. Note that the singularity, $[\cos^2\theta\,(k^2-u^2-v^2)]^{-1}$, in (4.4) and (4.5) is due to the assumption of a perfectly conducting surface. It comes from taking the limit as ε_r tends to infinity on the following factor

$$\left| \frac{(\varepsilon_r-1)^2(\varepsilon_r-\sin^2\theta)^{1/2}}{[\varepsilon_r\cos\theta+(\varepsilon_r-\sin^2\theta)^{1/2}][\cos\theta+(\varepsilon_r-\sin^2\theta)^{1/2}]} \right|^2 \left| \varepsilon_r(k^2-u^2-v^2)^{1/2}+(\varepsilon_r k^2-u^2-v^2)^{1/2} \right|^{-2}$$

while keeping $(k^2-u^2-v^2)^{-1/2}$ greater than zero. The dielectric formulation given above [Valenzuela, 1967] does not have a singularity when $(k^2-u^2-v^2)^{-1/2}$ tends to zero. Thus, in actual evaluation we should use the dielectric expression with a large enough ε_r. Figure 4.1 illustrates the convergence of σ^o_{VH} in ε_r. It shows that when the relative dielectric constant is larger than 10000, the surface acts like a perfectly conducting surface in its scattering behavior.

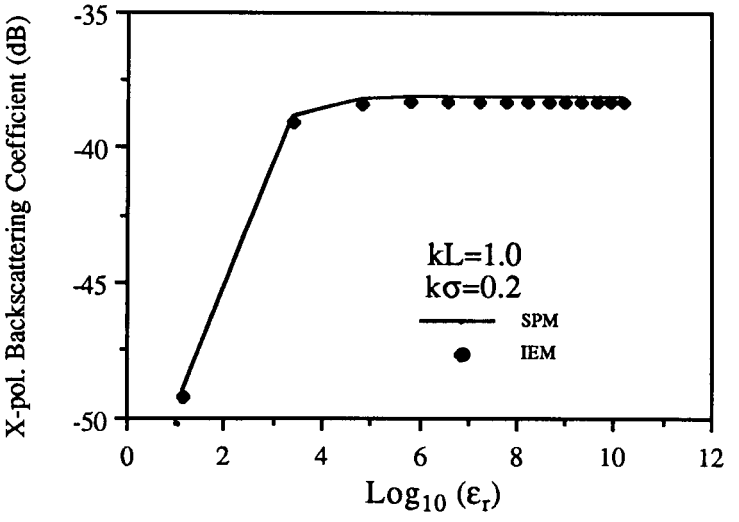

Figure 4.1 The convergence of IEM with ε_r

4.2 Theoretical Results

For ease of reference we shall refer to (4.1) and (4.4) as the Integral Equation Model (IEM) since it is based on the integral equation for the surface current. In Figures 4.2 through 4.5 we show the dependence of the like and cross-polarization coefficients on the roughness parameter $k\sigma$ between 0.25 and 1.0 while kL is kept constant at 3.14. We purposely select an intermediate kL value since in the low and high frequency regions, scattering characteristics can be easily determined from the small perturbation and the Kirchhoff models. For the purpose of obtaining some reference, the predictions of the Kirchhoff and the first-order small perturbation models in like-polarization and the second-order perturbation in cross-polarization are also plotted on the same graphs. At $k\sigma = 0.25$ IEM predictions agree well with the small perturbation results in cross-polarization but deviate at larger angles of incidence in like-polarizations because the kL value is larger than what is required by the perturbation model. The Kirchhoff predictions are correct only at normal incidence.

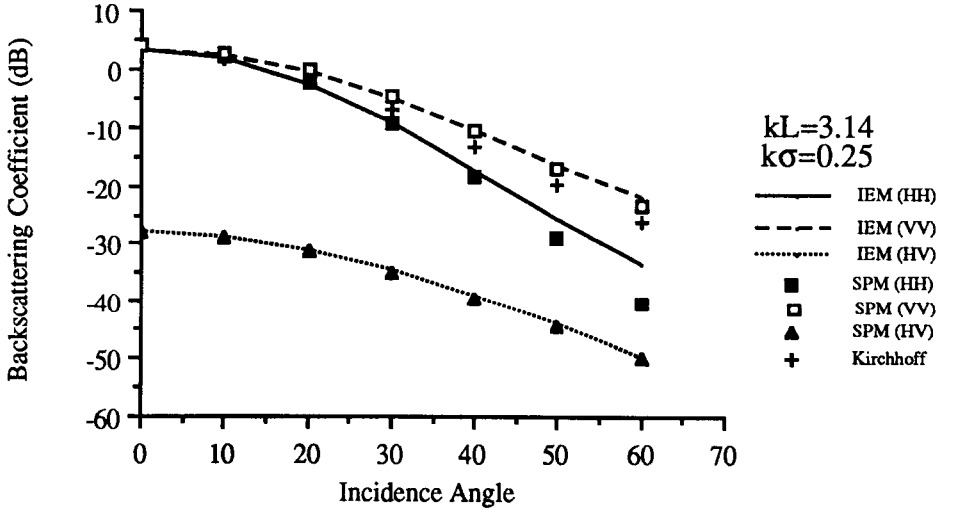

Figure 4.2 Comparison of the backscattering coefficient for both like and cross-polarizations among IEM, Kirchhoff, and small perturbation models. The normalized roughness parameters of the surface are $k\sigma$=0.25 and kL=3.14.

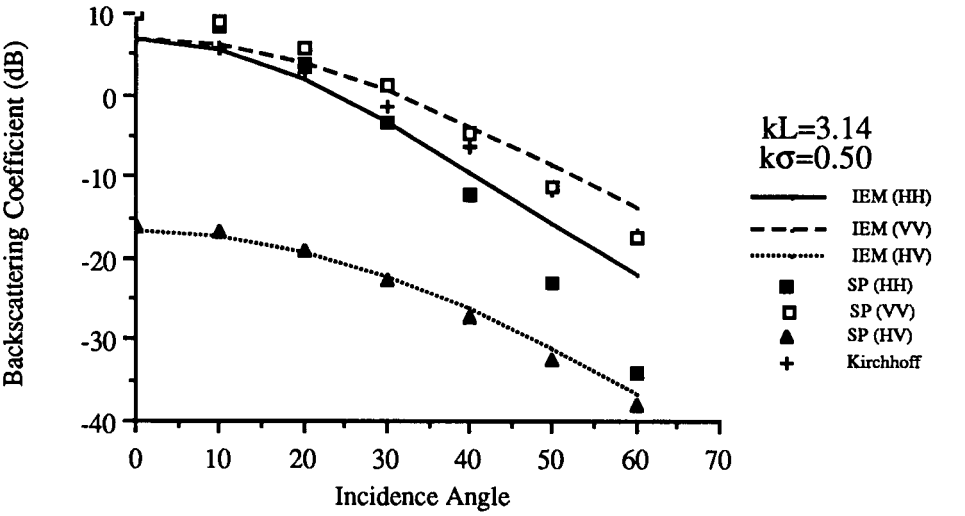

Figure 4.3 Comparison of the backscattering coefficient for both like and cross-polarizations among IEM, Kirchhoff, and small perturbation models. The normalized roughness parameters of the surface are kσ=0.50 and kL=3.14.

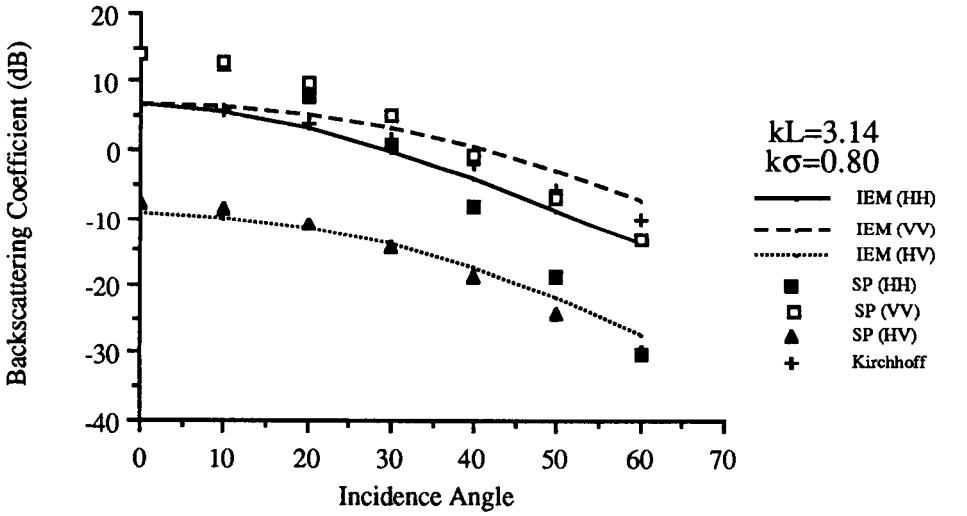

Figure 4.4 Comparison of the backscattering coefficient for both like and cross-polarizations among IEM, Kirchhoff, and small perturbation models. The normalized roughness parameters of the surface are kσ=0.80 and kL=3.14.

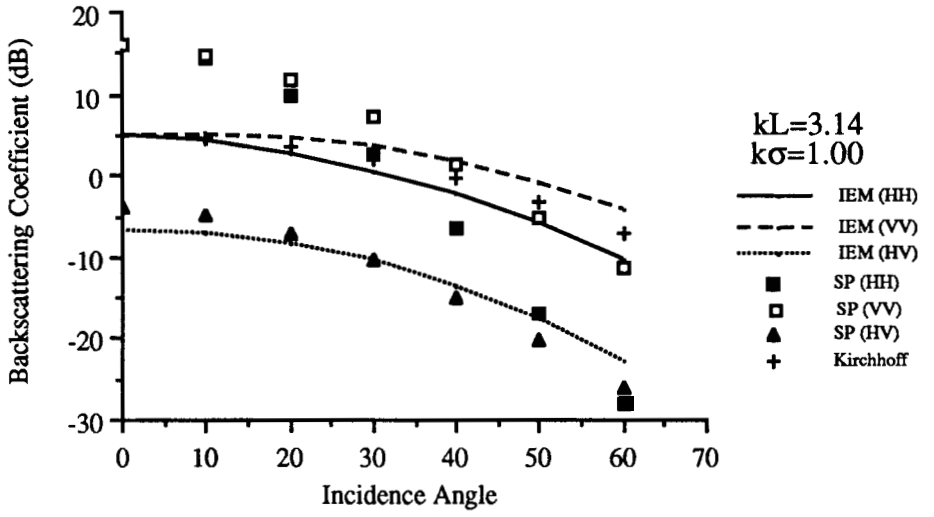

Figure 4.5 Comparison of the backscattering coefficient for both like and cross-polarizations among IEM, Kirchhoff, and small perturbation models. The normalized roughness parameters of the surface are $k\sigma$=1.0 and kL=3.14.

As $k\sigma$ increases to 0.5, IEM predictions differ significantly from the small perturbation results in like-polarizations since the latter is no longer valid. The cross-polarized returns have also begun to differ, but not significantly. This shows that the cross-polarized coefficient given by the second-order perturbation method has a wider range of validity in kL and $k\sigma$ values than the first-order like-polarized coefficients. As $k\sigma$ increases further to 0.8 and 1.0, the differences in cross-polarized scattering become more significant and it is clear that the second-order small perturbation model predicts a faster drop-off angular trend than the IEM. In all cases shown the Kirchhoff model predictions for like-polarizations continue to lie in between IEM predictions. The overall angular trends for both like and cross are to drop off slower as $k\sigma$ increases, and the level increase in the cross is much faster than the like.

Figures 4.6 through 4.9 show the IEM model behavior when the roughness parameter kL is varied from 1 to 6 while $k\sigma$ is kept at 0.2. In these graphs it is seen that for $k\sigma$ = 0.2 and kL = 1 IEM agrees well with the small perturbation model in both like and cross-polarizations. As kL increases, the separation between VV and HH polarizations decreases, angular trends drop off faster, and IEM approaches the

Kirchhoff model in like-polarization. Due to the choice of the small kσ value, the difference between the cross-polarized coefficients is not very significant even when kL is 6. This again shows that the second-order perturbation model for the cross-polarization has a wider range of validity than the first-order like-polarized model. Theoretically, this is to be expected. It is especially interesting to note that the level of the cross-polarized returns rises as kL increases from 1 to 3, but it then decreases for further increases in kL to lower levels than when kL was 1. The initial increase in level is due to having a larger scale of roughness, while the decrease is due to having a significantly smaller slope. This decrease is consistent with the fact that a Kirchhoff-type surface has a low level of depolarization.

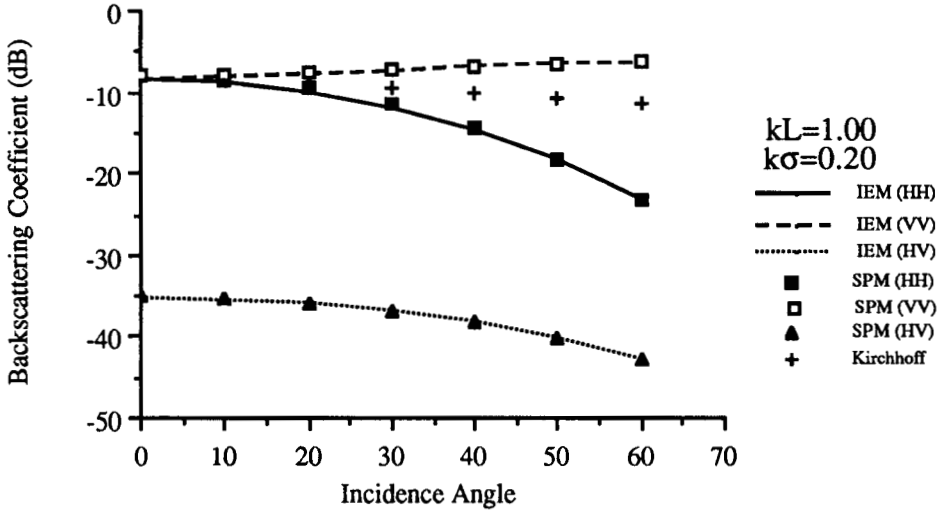

Figure 4.6 Comparison of the backscattering coefficient for both like and cross-polarizations among IEM, Kirchhoff, and small perturbation models. The normalized roughness parameters of the surface are kσ=0.2 and kL=1.0.

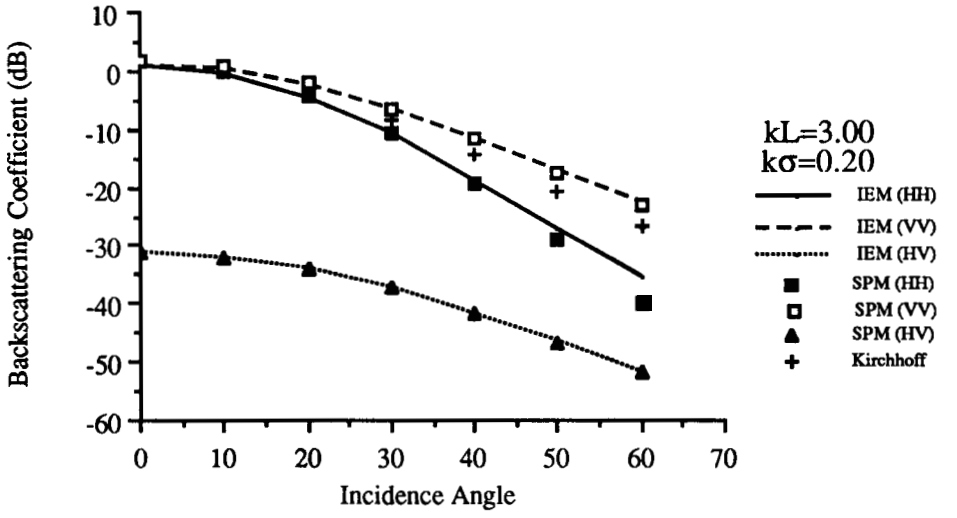

Figure 4.7 Comparison of the backscattering coefficient for both like and cross-polarizations among IEM, Kirchhoff, and small perturbation models. The normalized roughness parameters of the surface are kσ=0.2 and kL=3.0.

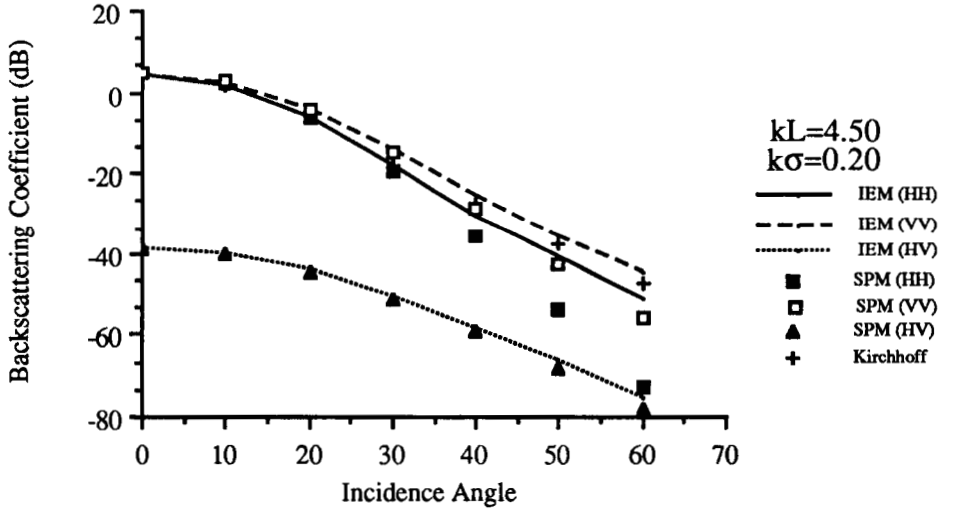

Figure 4.8 Comparison of the backscattering coefficient for both like and cross-polarizations among IEM, Kirchhoff, and small perturbation models. The normalized roughness parameters of the surface are kσ=0.2 and kL=4.5.

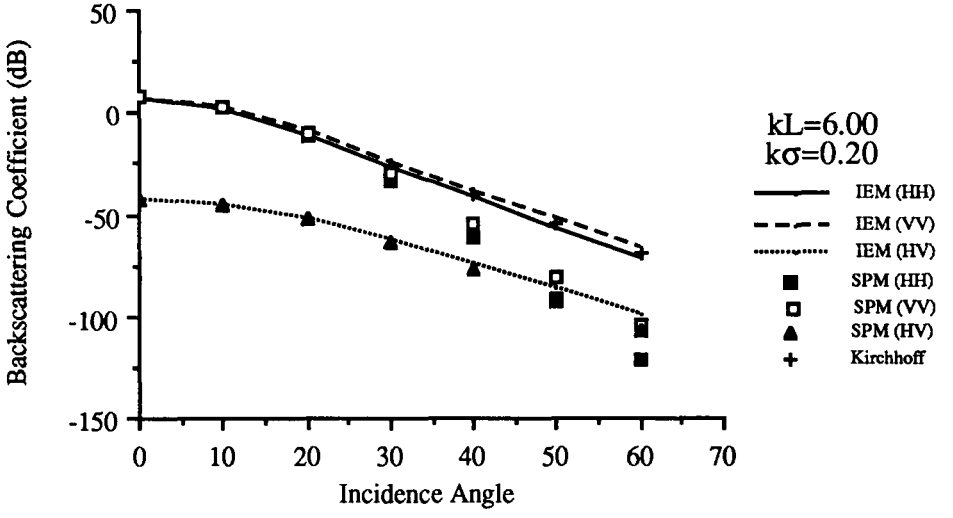

Figure 4.9 Comparison of the backscattering coefficient for both like and cross-polarizations among IEM, Kirchhoff, and small perturbation models. The normalized roughness parameters of the surface are $k\sigma$=0.2 and kL=6.0.

In Figures 4.10 through 4.13 we repeat the same calculations as in Figures 4.6 to 4.9 for $k\sigma$=1.0. In this case differences in level and angular trends are evident between the Kirchhoff, the small perturbation, and the IEM in both like and cross-polarizations. As in Figures 4.6 to 4.9, an increase in kL leads to smaller surface slopes and curvatures thus permitting better agreement between IEM and the Kirchhoff model in like-polarization. While the second-order perturbation estimate of the cross-polarized return does differ in every case from IEM due to the choice of $k\sigma = 1$, they are in better agreement when kL is larger because the surface is smoother.

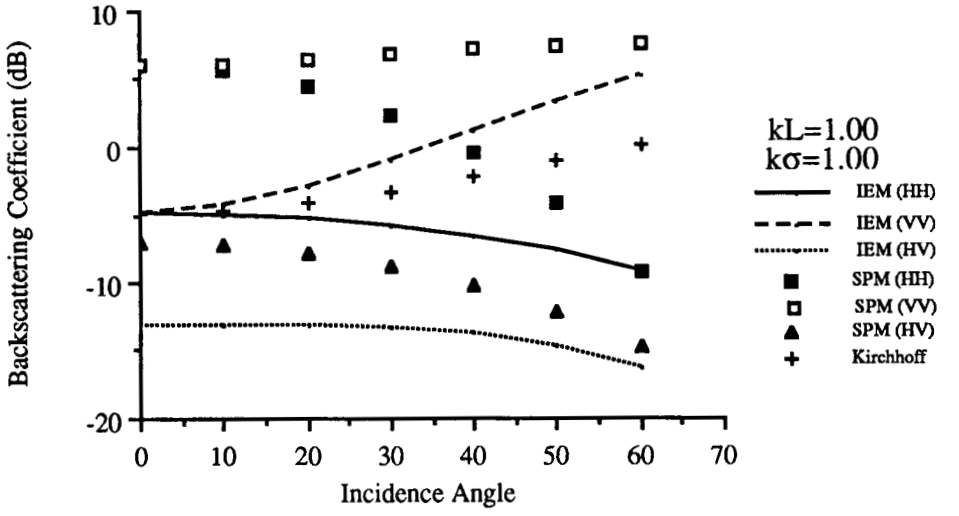

Figure 4.10 Comparison of the backscattering coefficient for both like and cross-polarizations among IEM, Kirchhoff, and small perturbation models. The normalized roughness parameters of the surface are kσ=1.0 and kL=1.0.

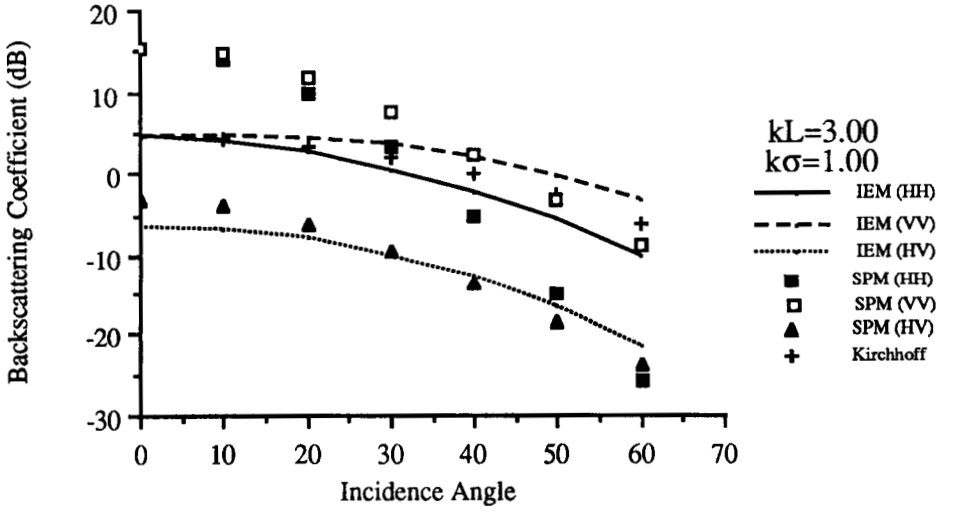

Figure 4.11 Comparison of the backscattering coefficient for both like and cross-polarizations among IEM, Kirchhoff, and small perturbation models. The normalized roughness parameters of the surface are kσ=1.0 and kL=3.0.

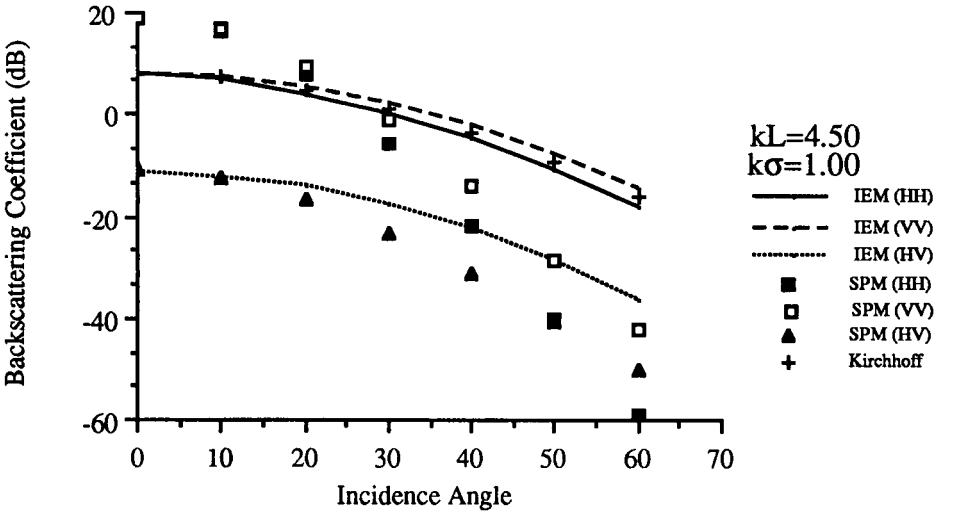

Figure 4.12 Comparison of the backscattering coefficient for both like and cross-polarizations among IEM, Kirchhoff, and small perturbation models. The normalized roughness parameters of the surface are kσ=1.0 and kL=4.5.

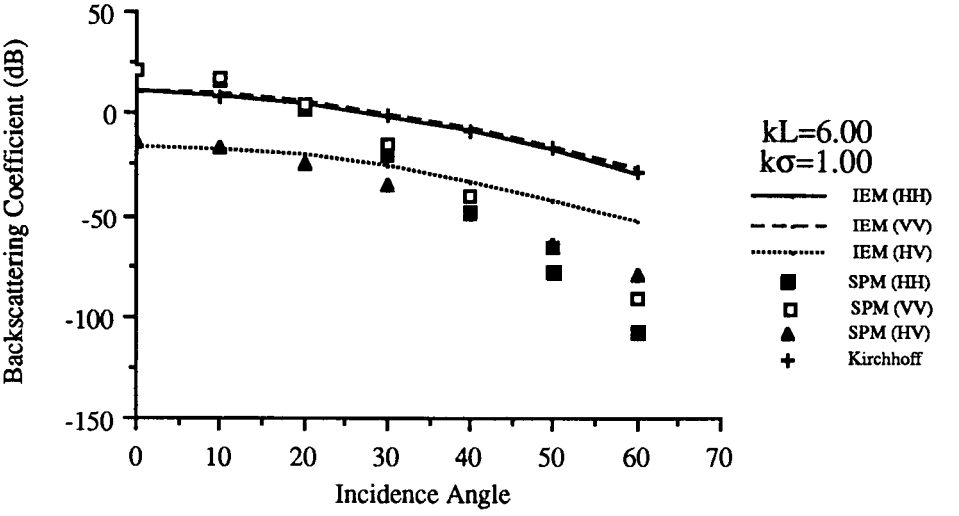

Figure 4.13 Comparison of the backscattering coefficient for both like and cross-polarizations among IEM, Kirchhoff, and small perturbation models. The normalized roughness parameters of the surface are kσ=1.0 and kL=6.0.

To show frequency dependence we illustrate in Figures 4.14 to 4.17 the like-polarized scattering properties by varying kσ from 0.125 to 1 and kL from 0.75 to 6, a change in frequency by a factor of 8. We see a gradual decrease in the separation between the VV and HH polarizations, a fast increase in the level of the backscattering coefficients in the low frequency region, a gradually faster angular drop off, and the approach to the geometric optics solution at the high frequency end. In the meantime it is seen that both like and cross-polarized returns agree with the perturbation solution at the low frequency end. Then, as frequency increases, the like-polarized coefficients begin to deviate from the perturbation solution first, and then the cross-polarized coefficient. Note that while the polarized coefficients approach the Kirchhoff solution at the high frequency end just like the case when kL increases, the cross-polarized coefficient near vertical incidence appears to saturate at the high frequency end. The difference in the cross-polarized behavior between large kL and high frequency cases is due to the fact that the surface does not change in the study of the frequency response, while permitting kL to increase means that the surface slope is becoming smaller.

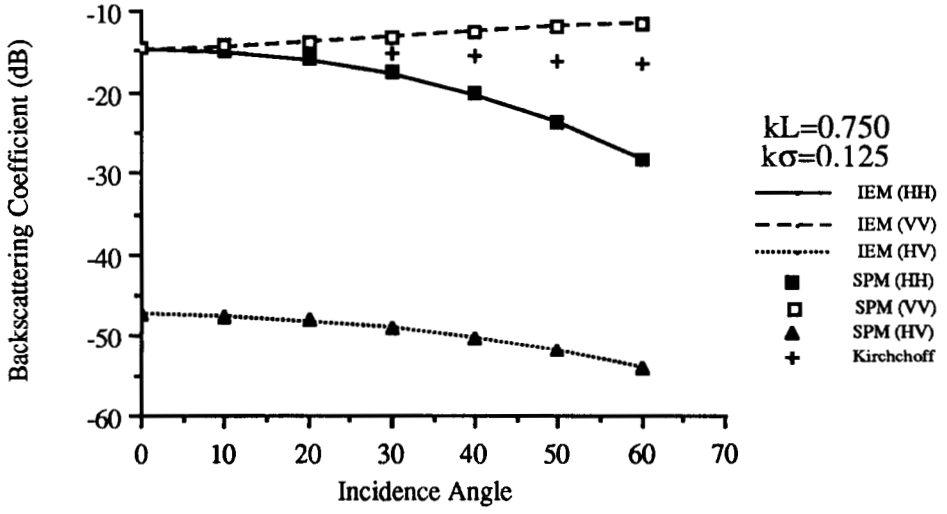

Figure 4.14 Comparison of the backscattering coefficient for both like and cross-polarizations among IEM, Kirchhoff, and small perturbation models. The normalized roughness parameters of the surface are kσ=0.125 and kL=0.75.

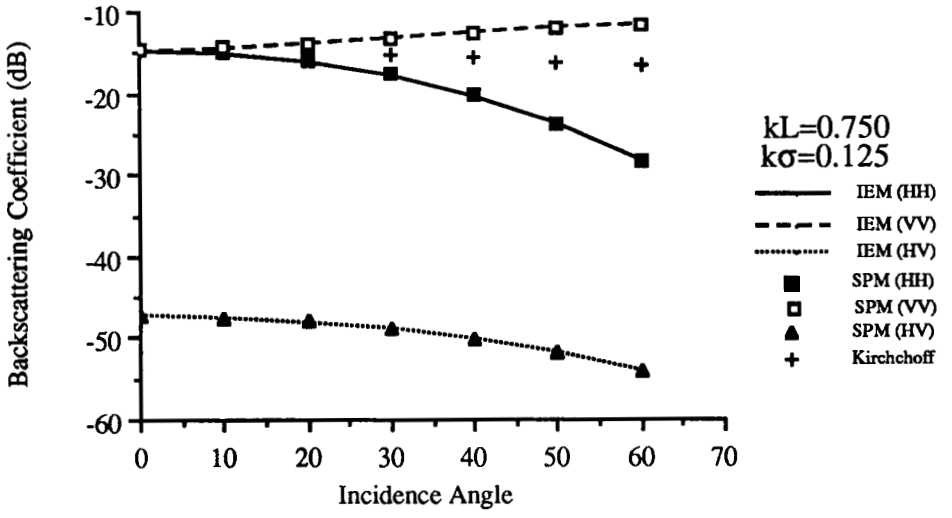

Figure 4.15 Comparison of the backscattering coefficient for both like and cross-polarizations among IEM, Kirchhoff and small perturbation models. The normalized roughness parameters of the surface are kσ=0.5 and kL=3.0.

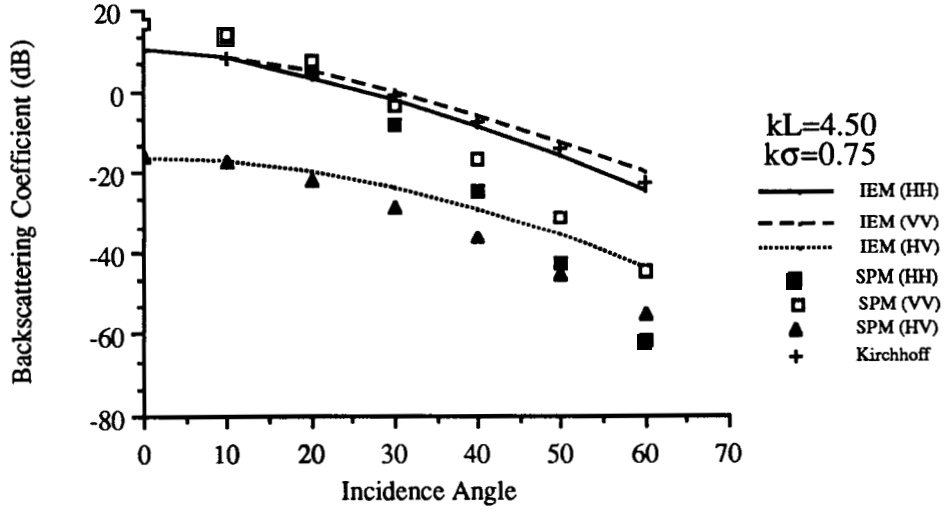

Figure 4.16 Comparison of the backscattering coefficient for both like and cross-polarizations among IEM, Kirchhoff, and small perturbation models. The normalized roughness parameters of the surface are kσ=0.75 and kL=4.50.

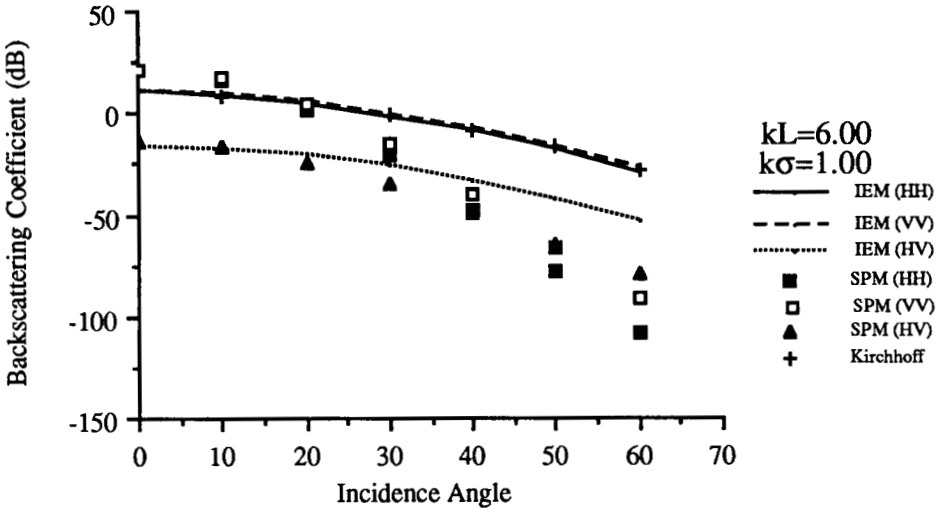

Figure 4.17 Comparison of the backscattering coefficient for both like and cross-polarizations among IEM, Kirchhoff, and small perturbation models. The normalized roughness parameters of the surface are $k\sigma=1.00$ and $kL=6.0$.

5. DISCUSSIONS

Significant progresses have been made in the surface scattering modeling and a new approach in generating a known randomly rough surface has been developed. At this point in time sufficient data have not been gathered to validate the scattering model. This will be carried out in the future.

In the past the Percus-Yevich's pair correlation function, which was based on microscopic considerations, was used in the dense medium scattering model and, hence, the correlation function does not contain the correlation length parameter. An independent approach to develop a dense medium scattering model based on macroscopic considerations has been performed, which leads to a correlation function with its correlation length depending on scatterer dimensions. This model will be used to interpret field measurements. To verify the scattering it is necessary to perform experiments on well controlled dense media with a variable volume fraction. This is

yet to be done. The use of the field data alone does not provide enough cases and as detailed a ground truth to verify a scattering model.

In conclusion, the most urgently needed results are complete sets of measurements from known surface and volume targets covering a range of target parameters over a wide range of frequencies, angles, and polarizations. We believe that scattering models must be compared with measurements from both data collected in the field, and data collected from known targets, to establish their applicability.

REFERENCES

Rice, S.O., "Reflection of Electromagnetic Waves from Slightly Rough Surfaces," *Communications in Pure and Applied Mathematics*, Vol. 4, No. 213, pp. 361-378, 1951.

Valenzuela, G.R., "Depolarization of EM Waves by Slightly Rough Surfaces," *IEEE Transactions Antenna and Propagation*, Vol. AP-15, No. 4, pp. 552-557, 1967.

Ulaby, F.T., Moore, R.K. and Fung, A.K., "Microwave Remote Sensing: Active and Passive," Vol. 2, Chapter 12, Artech House, 1982.

Fung, A.K. and Pan, G.W., "The Integral Equation Method for Rough Surface Scattering," *Proceeding of Multiple Scattering from Random Media and Randomly Rough Surfaces*, Pennsylvania State University, 1985.

Karam, M.A. and Fung, A.K., "Radiative Transfer in Multilayered Random Medium with Laminar Structure: Green's Function Approach," *Journal of Applied Physics*, Vol. 59, No. 11, pp. 3650-3661, June 1986.

Fung, A.K. and Pan, G.W., "A Scattering Model for Perfectly Conducting Random Surfaces: Part I. Model Development," *International Journal of Remote Sensing,* Vol. 8, No. 11, pp. 1579-1593, 1987.

Pan, G.W. and Fung, A.K., "A Scattering Model for Perfectly Conducting Random Surfaces: Part II. Range of Validity," *International Journal of Remote Sensing,* Vol. 8, No. 11, pp. 1595-1605, 1987.

Fung, A.K., Chen, M.F. and Lee, K.K., "Fresnel Field Interaction Applied to Scattering from a Vegetation Layer," *Remote Sensing of Environment*, Vol. 23, No. 1, pp. 35-50, October 1987.

Zhu, P.Y., Fung, A.K. and Wong, K.W., "Effective Propagation Constants in Dense Random Media Under Effective Medium Approximation," *Radio Science*, Vol. 22, No. 2, pp. 234-250, 1987.

Fung, A.K. and Chen, M.F., "Modeling of Microwave Emission and Scattering from Snow and Soil," Cospar Committee on Space Research, July 18-29, Espoo, Finland, 1988.

Blanchard, A.J. and Nance, C.E., "Bistatic Microwave Measurements of Simulated Natural Structures," *Journal of Wave-Material Interaction*, Vol. 3, No. 2, April 4-8, 1988.

Fung, A.K., "Scattering Models for Radar Image Simulation," *Proceedings of the EARREL Workshop, Sar Simulation Models,* pp. 52-69, Capri (Naples), Italy, May 1988.

Rochier, J.D., Blanchard, A.J. and Chen, M.F., "The Generation of Surface Targets with Specified Surface Statistics," *International Journal of Remote Sensing*, July 1988.

Karam, M.A., Fung, A.K., Blanchard, A.J. and Shen, G.X., "The Leaf Shape Effect on Electromagnetic Scattering from Vegetated Media," *Digest of the International Geoscience and Remote Sensing Symposium,* (IGARSS '88), University of Edinburgh, Scotland, UK, September 13-16, 1988a.

Karam, M.A., Fung, A.K., Blanchard, A.J. and Nance, C.E., "The Extinction Properties of Forest Components," *Proceedings of the International Geoscience and Remote Sensing Symposium,*(IGARSS '88), University of Edinburgh, Scotland, UK, September 13-16, 1988b.

Karam, M.A. and Fung, A.K., "Electromagnetic Scattering from a Layer of Finite Length, Randomly Oriented Dielectric Circular Cylinders Over a Rough Interface with Application to Vegetation," *International Journal of Remote Sensing*, Vol. 9, No. 6, pp. 1109-1134, 1988.

Liu, H.L. and Fung, A.K., "An Empirical Model for Polarized and Cross-Polarized Scattering from a Vegetation Layer," *Remote Sensing of Environment*, Vol. 25, pp. 23-36, 1988.

Nance, C.E., Blanchard, A.J. and Chen, M.F., "Polarimetric Microwave Scattering from Known Randomly Rough Surfaces," *Proceedings of the International Geoscience and Remote Sensing Symposium,*University of Edinburgh, Scotland, UK, September 13-16, 1988.

Syed, I., Blanchard, A.J. and Fung, A.K., "Attenuation and Scattering Measurements from Dense Media," *Proceedings of the International Geoscience and Remote Sensing Symposium,*University of Edinburgh, Scotland, UK, September 13-16, 1988.

Karam, M.A., Fung, A.K., Antar, Y.M.M., "Electromagnetic Wave Scattering from Some Vegetation Samples," *IEEE Transactions on Geoscience and Remote Sensing*, Vol. 26, No. 6, pp. 113-122, November 1988c.

Karam, M.A. and Fung, A.K., "Radiative Transfer Theory for Active Remote Sensing of a Forested Canopy," *Digest of the International Geoscience Remote Sensing Symposium,* (IGARSS '89), submitted for publication, July 1989a.

Karam, M.A. and Fung, A.K., "Leaf Shape Effects in Electromagnetic Wave Scattering from Vegetation," *IEEE Transactions on Geoscience and Remote Sensing,* submitted for publication, 1989b.

Karam, M.A. and Fung, A.K., "The Extinction Properties of Forest Components," *International Journal of Remote Sensing,* submitted for publication, 1989c.

Karam, M.A. and Fung, A.K., "Electromagnetic Wave Extinction Within a Forested Canopy," *Digest of the International Geoscience Remote Sensing Symposium,* (IGARSS '89), submitted for publication, July 1989c.